MHD Studies in MAST

SD Pinches 1), RJ Akers 1), LC Appel 1), RJ Buttery 1), I Chapman 1), NJ Conway 1), G Cunningham 1), MP Gryaznevich 1), TC Hender 1), DF Howell 1), GTA Huysmans 2), R Martin 1), SE Sharapov 1) and the MAST and NBI Teams

1) Euratom/UKAEA Fusion Association, Culham Science Centre, Abingdon, OX14 3DB, UK
2) CEA-Cadarache, Association Euratom-CEA, 13108 St Paul-lez-Durance, France

e-mail contact of main author: Simon.Pinches@jet.efda.org

Abstract. The tight aspect ratio tokamak with its high-β capacity allows for an increased understanding of MHD stability, including, but not limited to, aspect ratio effects. The MAST tokamak is equipped with neutral beam injection (NBI) heating, a range of excellent diagnostics and external error field correction coils that allow non-axisymmetric (dominantly $n = 1$) fields to be applied. MAST has made considerable progress in studying sawtooth behaviour with co and counter-NBI, in observations of fast ion instabilities and on studies of the threshold for error field locked modes, as reported in this paper.

1. Introduction

Present day spherical tokamaks [1] with unbalanced tangential neutral beam injection (NBI) are capable of generating toroidal flows approaching the ion sound speed. Such high plasma rotation means that effects such as centrifugal forces become important when considering the stability of magnetohydrodynamic (MHD) modes such as the $n = 1$ internal kink mode. Here the MHD stability analysis code, MISHKA-F [2] is used to model the effect of toroidal flows on the ideal $n = 1$ internal kink mode.

Small asymmetries in the otherwise axisymmetric magnetic field configuration referred to as error fields are known to be able to stop the plasma rotating, drive resistive tearing modes and lead to disruptions. Correcting out these imperfections in the magnetic field using the error field correction coils on MAST has allowed MAST to operate at densities 30% lower than previously. Furthermore, studies looking at the error field necessary to induce mode locking have shown that the locked mode threshold in MAST scales in a similar way to that in conventional aspect-ratio tokamaks.

The low magnetic field in MAST means that the fast ion population resulting from NBI is super-Alfvénic. Indeed the fast ion drive of linear eigenmodes supported by the thermal plasma may be so strong that they start to exhibit highly nonlinear behaviour and so-called energetic particles modes may be created. This paper reports upon observations of shear Alfvén waves associated with a minimum in the magnetic shear: Alfvén Cascades (ACs). Two approaches for forming such reversed magnetic shear profiles have been identified and the existence of these ACs long into the current flat-top phase of the pulse provides evidence for the sustainment of the configuration.

2. Effects of toroidal flow on sawteeth

The sawtooth behaviour in MAST plasmas has been compared across approximately matched discharges with similar flat-top current, magnetic field and plasma shape. Since MAST is a tight aspect-ratio spherical tokamak, $a/R \simeq 0.7$, it has a low moment of inertia which when combined with a high power neutrally injected beam, results in rotation speeds significantly

higher than presented in previous JET results [3].

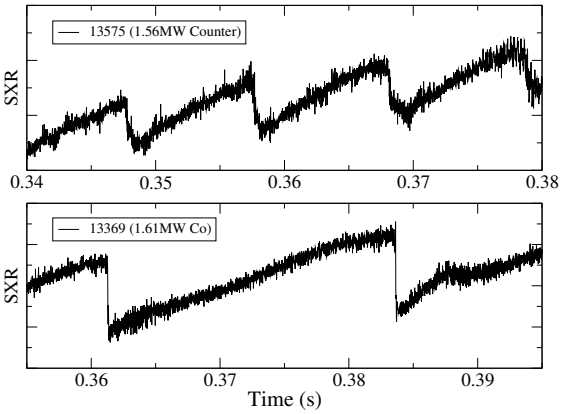

FIG. 1. Soft X-ray emission for two approximately identical MAST discharges with similar beam power injected in opposite directions. The sawtooth period is significantly longer when the NBI is oriented in the co-current direction.

Fig. 1 shows the soft X-ray traces from two shots in MAST with similar injected beam power but oriented in opposite directions. At the time of the first sawtooth crash, in shot 13575, $I_p = 719\,\mathrm{kA}$, $B_T = 0.36\,\mathrm{T}$ and $\bar{n}_e = 2.24 \times 10^{20}\mathrm{m}^{-3}$ whilst in discharge 13369, $I_p = 723\,\mathrm{kA}$, $B_T = 0.4\,\mathrm{T}$ and $\bar{n}_e = 2.26 \times 10^{20}\,\mathrm{m}^{-3}$. The NBI directed in the co-current direction (discharge 13369) results in a quiescent time which is over twice as long as that when the NB is injected in the counter-current direction. Fig. 2 shows the sawtooth period from a collection of shots which conform to the following parameter ranges: $I_p \in [680,740]\,\mathrm{kA}$, $B_T \in [0.35,0.45]\,\mathrm{T}$ and $\overline{n}_e \in [1.6,2.2] \times 10^{20}\,\mathrm{m}^{-3}$. Here the convention is used that negative beam power means injected in the counter-I_p direction whereas positive power is injected in the co-I_p direction. It is found that as the co-NBI is increased in MAST, the sawtooth period also increases. Conversely, as the counter-NBI is increased, the quiescent time decreases until the sawtooth period reaches a minimum, and then subsequently lengthens, analogous to the co-NBI regime. It is evident that for counter-NBI powers up to 1.5MW the sawtooth period is comparable to, or shorter than, typical Ohmic heating sawtooth periods ($\tau_{ST}^{Ohmic} \sim 10-15\,\mathrm{ms}$). The results obtained are consistent with those from JET [3].

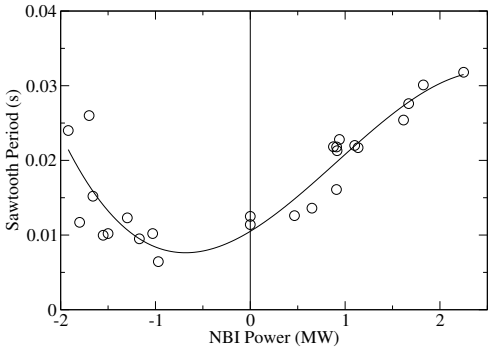

FIG. 2. Sawtooth period for MAST discharges as a function of applied NBI Power. $I_p \in [680,740]\,kA$, $B_T \in [0.35,0.45]\,T$ and $\overline{n}_e \in [1.6,2.2] \times 10^{20}\,m^{-3}$. Here the convention is used that negative beam power means injected in the counter-I_p direction whereas positive power is injected in the co-I_p direction

The linear stability of the ideal $n = 1$ internal kink mode with respect to the toroidal rotation at finite ion diamagnetic frequency has been analysed using the MISHKA-F code. MISHKA-F incorporates the effects of toroidal rotation and the ion diamagnetic drift on ideal and resistive eigenmodes in general toroidal geometry. It takes input from HELENA [6] which solves the static Grad-Shafranov equation which is sufficient as long as the toroidal rotation is sufficiently sub-sonic, $v_\phi/v_A < 0.2$ [7] where v_ϕ is the toroidal flow prescribed as a profile input to MISHKA-F, $v_A = B/\sqrt{\mu_0 n_0 M_i}$, B is the equilibrium magnetic field, n_0 is the plasma density and M_i is the mass of the ions. The growth rate of the kink mode is decreased as the toroidal rotation is increased in the co-current direction. However, when there is a finite ion diamagnetic frequency, the $n = 1$ internal kink mode is initially destabilised by toroidal rotation in the counter-ω_{*i} direction, before being completely stabilised at high toroidal flows. This is consistent with the results found experimentally in MAST.

Fig. 3 shows the growth rate of the $n = 1$ internal kink mode in discharge 13541 with respect to the rotation velocity at the magnetic axis. As the ion diamagnetic frequency is increased,

the toroidal rotation velocity at which the $n = 1$ internal kink mode is most unstable increases in the counter-ω_{*i} direction. When modelled at the same ion diamagnetic frequency as measured experimentally at the time of the first sawtooth crash, it is found that the kink mode is most unstable at approximately the same toroidal velocity that minimised the sawtooth period experimentally (see Fig. 4).

The sawtooth period is an inherently non-linear property, so in order to use linear stability analysis to address this it is necessary to consider the radial location of the $q = 1$ surface amongst other effects. The $q = 1$ surface increases radially as a function of time [4] between sawtooth crashes, meaning that the position of the $q = 1$ surface is related to the sawtooth period. As q_0 is increased towards unity, the position of the $q = 1$ surface moves radially inwards, since the q-profile is monotonically increasing. When q_0 is varied in MISHKA-F, the toroidal magnetic field is scaled but the poloidal beta value remains at the experimental value, $\beta_p = 0.56$. The marginally stable $q = 1$ position with respect to the toroidal rotation speed at the $q = 1$ surface is plotted in Fig. 4.

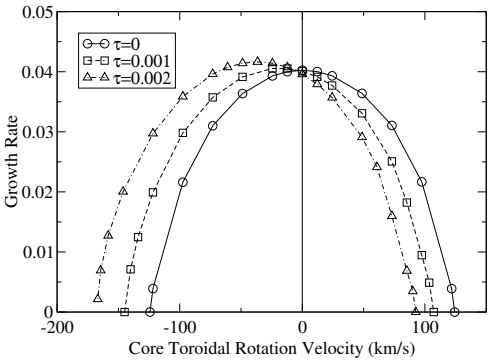

FIG. 3. The growth rate of the ideal $n = 1$ internal kink mode in discharge 13541 as a function of the toroidal rotation speed. The parameter τ represents the ion diamagnetic frequency.

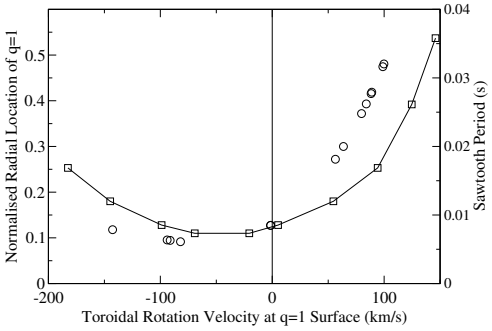

FIG. 4. The radial location of the marginally stable $q = 1$ surface in discharge 13541 with respect to the toroidal rotation at the resonant surface (squares). Also shown for comparison is the sawtooth period of shots in MAST (open circles). It should be noted that the discharges with no NBI heating are marginally ideally stable and require a ramp in β to drive $n = 1$ internal kink instabilities.

The scans represented in this figure are for the $n = 1$ internal kink mode in counter-NBI discharge 13541 using the experimental rotation profile and ion diamagnetic frequency, $\omega_{*i} = 23\,\mathrm{kHz}$. The $q = 1$ surface is nearest to the centre at approximately the same counter-v_ϕ as required to minimise the sawtooth period. Using the assumption that $r|_{q=1} \propto \tau_{ST}$ this suggests good accordance between the MISHKA-F stability analyses and the experimental data from MAST.

Analytically, the growth rate of the internal kink mode as a function of the toroidal velocity can be found by using Eq. (3.17) of Ref. [5]:

$$\Omega = \frac{\omega_{*i}}{2} \pm \frac{1}{2}(1-\kappa^2)^{1/2}[\omega_{*i}^2 - 4(1-\kappa^2)\Lambda^2\omega_A^2]^{1/2} \quad (1)$$

where Ω is the Doppler shifted mode frequency, $\Omega = \omega - v_E(r_0)k_y$, ω is the mode frequency, v_E is the $E \times B$ drift speed, ω_{*i} is the ion diamagnetic frequency and $\Lambda = qR\hat{\gamma}/v_A s$, with

$$\hat{\gamma}^2 = -\frac{1}{(1-\kappa^2)^2}\left[\Omega(\Omega - \omega_{*i}) + \frac{\kappa^2\omega_{*i}^2}{4}\right]. \quad (2)$$

The dimensionless parameter κ is the normalised velocity shear,

$$\kappa = \frac{qR}{sv_A}\frac{\mathrm{d}}{\mathrm{d}r}\left(\frac{rv_\phi}{Rq}\right), \quad (3)$$

where $k_y = m/r$, m is the poloidal mode number and s is the magnetic shear, $s = (r/q)dq/dr$, evaluated at the $q = 1$ surface. In these studies, the κ terms will be small since the toroidal velocity shear is much smaller than the Alfvén frequency and the magnetic shear is not very low. In the limit $v_\phi \ll v_A$ and $s \sim 1$, equation 1 becomes

$$\Omega \equiv \omega - \Omega_\phi \simeq \omega_{*i} \tag{4}$$

This means that the precursor mode frequency will change direction when $\Omega_\phi \simeq -\omega_{*i}$, which is to say that the toroidal rotation frequency of the plasma induced by the NBI balances the ion diamagnetic frequency. The results presented above are consistent with this theoretical prediction.

MHD stability analyses including toroidal rotation effects have accurately modelled experimental sawtooth behaviour on MAST. Such behaviour can be attributed to fluid effects [8] arising from the high toroidal flows generated by neutral beam injection. Kinetic modelling, which will be addressed in future work, will aim to assess the contribution made by kinetic effects [9] to the stabilisation of the kink mode.

3. Error fields

Non-axisymmetric magnetic fields, or error fields, which are caused by imperfections and misalignments of the field coils, have the potential to induce instabilities in the plasma which can stop the plasma rotation and terminate the discharge. A set of four error field correction coils have been installed on MAST to study this and enable a correcting magnetic field to be applied. Each coil consists of three turns and can carry a maximum current of 15 kA·turns of current. In routine use, the coils are arranged in two pairs, with opposite coils wired in series to produce non-axisymmetric magnetic fields with an odd-n spectrum.

Error fields play a particular role in the physics governing the β_N limit. This limit originates from the $n = 1$ kink mode, but can be increased by plasma rotation, which has a dissipative interaction with the kink mode in the presence of a wall. New modelling studies for MAST indicate that in-vessel conducting structures have a wall-like stabilising effect, opening up a window for operation above the no-wall kink mode β-limit. This indicates that the highest β_N discharges on MAST access this rotational stabilisation regime. Thus an upgrade to the neutral beam systems now leaves MAST well placed to probe this resistive wall mode physics, using its error field systems to perturb plasma rotation

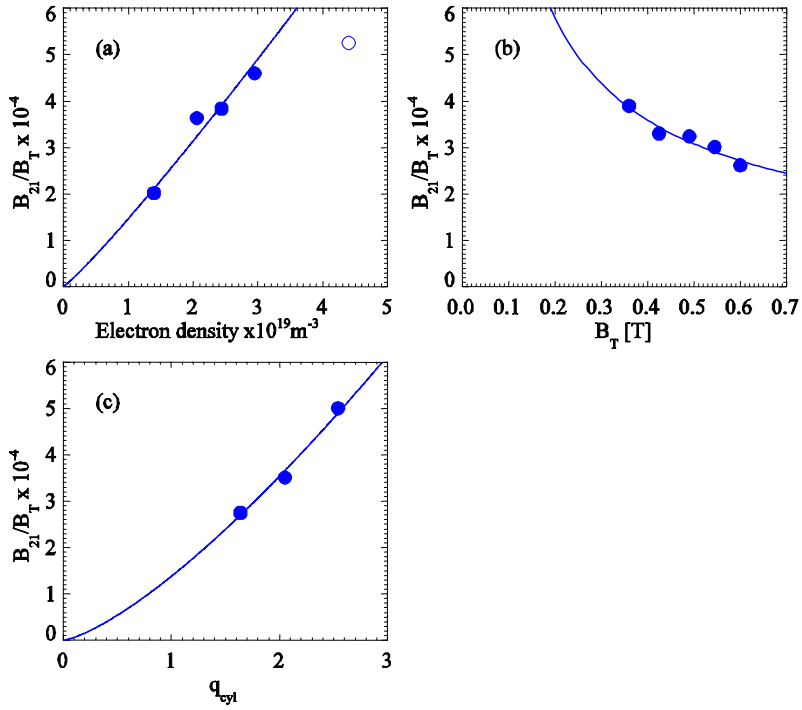

FIG. 5. Scaling of locked mode threshold with density, toroidal field and safety factor.

and test models for the dissipation mechanisms that stabilise the mode.

Three scans were performed in order to determine how the locked mode threshold scales with density, toroidal field and q. In each of the scans, one quantity was varied while the other two quantities were kept constant. Fig. 5 shows the results of the scans that were performed. The density scan, Fig. 5a, was performed at fixed $B_T = 0.55\,\mathrm{T}$, $I_p = 600\,\mathrm{kA}$. The open point had a different value of q_{95} than the rest of the dataset and so was not included in the fit. The toroidal field scan, Fig. 5b, was performed at fixed density, $n_e = 2.3 \times 10^{19}\,\mathrm{m}^{-3}$ with the ratio B_T/I_p fixed. The q scan, Fig. 5c, was performed at fixed density, $n_e = 2.2 \times 10^{19}\,\mathrm{m}^{-3}$ and $B_T = 0.6\,\mathrm{T}$ and q was varied by varying I_p. Here the scaling is presented as a function of the cylindrical q,

$$q_{cyl} = \frac{5a^2 B_T}{I_p R_{geom}},$$

where a is the minor radius in m, I_p is the plasma current in MA, B_T is the toroidal field in T at the geometric radius, R_{geom} which is in m. The full scaling is represented as a power law,

$$\frac{B_{21}}{B_T} = 5 \times 10^{-5} \overline{n}_e^{1.1\pm0.2} B_T^{-0.7\pm0.1} q_{cyl}^{1.4\pm0.2}$$

Here, B_{21} is the $m = 2$, $n = 1$ component of the applied magnetic field normal to the $q = 2$ surface.

By applying currents in the error field correction coils to cancel out the intrinsic error it has been possible to operate MAST in regimes that were not accessible without this correction, such as a low density regime used to study current drive physics. Fig. 6 shows a matched pair of shots where the density was reduced gradually through the shot. It can be seen that in the case where there was no error field correction (blue traces) a locked mode starts to grow from 210 ms. There is a sudden drop in density, the sawteeth disappear and the discharge disrupts at 260 ms. With error field correction (red traces) the discharge is seen to continue dropping in density, no locked mode is seen and the discharge runs to full length. By applying error field correction it was possible to achieve a density 30% lower than that achievable otherwise, and this density was still not low enough for a locked mode to occur.

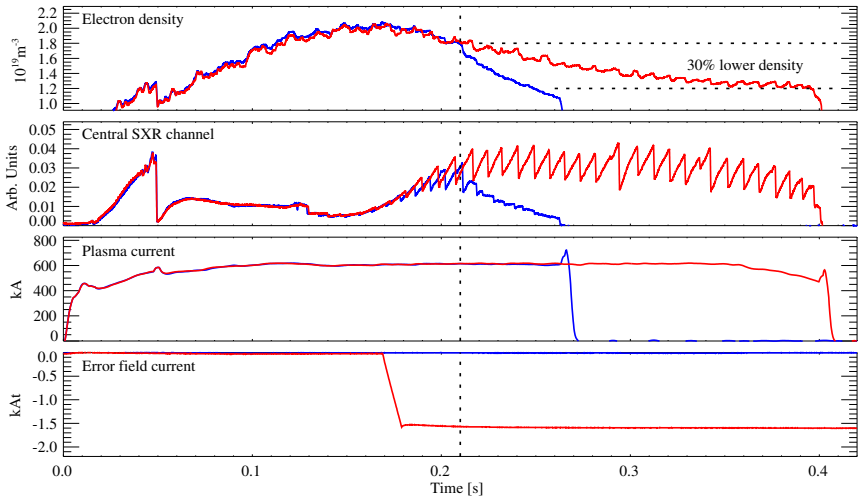

FIG. 6. Demonstration of error field correction increasing the operational space of the machine.

The power law scaling found above can be used to extrapolate to future devices, such as a proposed steady state spherical tokamak fusion power plant (STPP) [23] or component test facility (CTF) [24]. Using the scaling law found for MAST, these values give a locked mode threshold of $B_{21}/B_T = 1.85 \times 10^{-4}$ for the STPP and $B_{21}/B_T = 1.0 \times 10^{-4}$ for the CTF. When the uncertainties in the scaling law are taken into account, the locked mode threshold is predicted to be in the range $B_{21}/B_T \in [1.05, 3.3] \times 10^{-4}$ for the STPP and $B_{21}/B_T \in [0.55, 1.75] \times 10^{-4}$ for the

CTF. On MAST, the intrinsic error field B_{21}/B_T is of the order 1.3×10^{-4}. Therefore, it would be prudent to include a set of error field correction coils in the design of any future device.

4. Fast particles

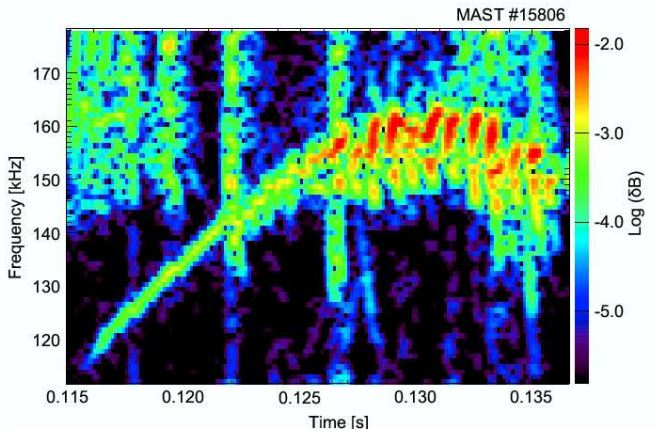

FIG. 7. Alfvén cascade in MAST discharge #15806. As the mode enters the TAE frequency gap it exhibits up-down frequency sweeping behaviour characteristic of the formation of holes and clumps [21].

Several types of Alfvénic instabilities including Toroidal Alfvén Eigenmodes (TAEs) can be excited on MAST through resonant interaction with the energetic ions produced by neutral beam injection (NBI). However, it was first noted that the NBI system drives these waves to such a strong degree that only high-amplitude "chirping" (frequency-sweeping) linear [22] and non-linear [10] non-perturbative modes are observed. A scan in NBI power from 1.5 MW down to 0.5 MW was therefore performed in order to reduce the energetic ion drive and avoid these chirping modes. It was found that the optimum NBI power required to drive clearly observable ACs was 1.3 MW. At this power, TAE are still highly unstable however and they generate double-chirping modes as shown in Fig. 7 and previously investigated in detail [10].

The Alfvén cascade (AC) eigenmode is a global shear Alfvén wave characteristic of "advanced" tokamak plasmas where a non-monotonic safety factor profile, $q(r)$, is present. These have been searched for, found, and investigated in a recent series of experiments conducted on MAST. ACs, as shown in Fig. 8, are associated with the extremum point of the Alfvén continuum localised at the magnetic surface where the minimum value of $q(r)$, labelled as q_{min}, occurs [12, 13, 14]. During the evolution of the plasma current, the eigenfrequency of the AC, $\omega_{AC}(t)$, changes due to the evolution of $q_{min}(t)$, via the dispersion relation for shear Alfvén waves,

$$\omega_{AC}(t) = \frac{v_A}{R_0}\left|n - \frac{m}{q_{min}(t)}\right| + \Delta\omega, \qquad (5)$$

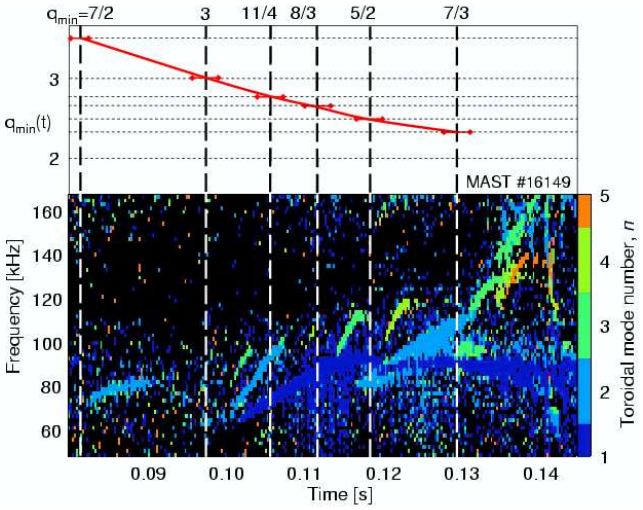

FIG. 8. Alfvén cascades in MAST discharge #16149. The colours indicate the toroidal mode number and enable the deterimination of $q_{min}(t)$. The simultaneous occurrence of all modes at $t \sim 100$ ms corresponds to $q_{min} = integer = 3$ and is known as a Grand Cascade.

and observations of ACs immediately reveal two important equilibrium properties, namely that the shear is reversed and the rate of current diffusion at the position of q_{min},

$$\frac{d}{dt}\omega_{AC}(t) \simeq m\frac{v_A}{R_0}\frac{d}{dt}q_{min}^{-1}(t). \qquad (6)$$

Previous observations of ACs with magnetic pick-up coils and interferometry have been made on JET [12, 13, 14, 15], DIII-D [16], JT-60U [17], TFTR [18], and C-MOD [19]. Due to

the simple and robust relation in equation (6) between the frequency of the observed AC and $q_{min}(t)$, and because of the time correlation between q_{min} = integer and internal transport barrier (ITB) triggering events in shear-reversed plasmas, ACs are routinely used for developing ITB scenarios on JET [15, 20] and DIII-D [16].

In addition to studying the physics of global shear Alfvén waves at tight aspect ratio, the search for Alfvén cascades on MAST also aimed at developing a reliable diagnostic for magnetic shear reversal. On MAST ACs were observed in two main scenarios. The first scenario had a fast (> 5 MA/s) ramp-up of the inductive current and NBI was applied early in the discharge, i.e. at 70 ms (see blue trace in Fig. 9). The second scenario undertook a two-step current ramp-up and NBI was applied late, at 150 ms (see red trace in Fig. 9).

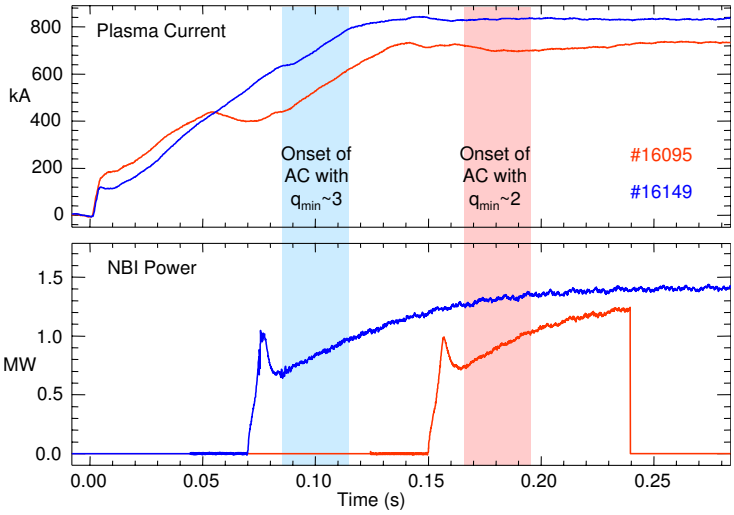

FIG. 9. Time traces showing time evolution of plasma current and neutral beam heating in MAST shots #16095 and #16149.

In the first scenario, ACs and ITBs associated with the magnetic surface $q_{min} = 3$ were investigated, whilst the second scenario aimed at studying ACs and ITBs at the time of $q_{min} = 2$ appearing in the plasma. Both scenarios supported ACs and, occasionally, ITBs, with the two-step scenario achieving temperatures approximately double that in the other scenario, $T_i \simeq T_e \simeq 1.2$ keV. After identifying the optimal NBI power, the start time of NBI was scanned in both scenarios to attain the most unambiguous AC observation for as long as possible. The best NBI time was found to be 70 ms in the first scenario and 130 ms in the second. In both cases, the ACs were observed until at least 220 ms into the discharge showing the existence of magnetic shear-reversal well into the current flat-top phase. In addition to being visible in the external magnetic measurements, ACs were also visible using the MAST interferometry system. In the second (two-stage current ramp-up) scenario described above, an increase of the current ramp-up rate during the second step was found to lead to significant MHD activity with no further evidence for a shear-reversed equilibrium. Only TAE modes and no ACs were subsequently observed. Following this event, a number of high-frequency modes (≤ 1 MHz) clustered in frequency were detected using the new high-frequency magnetic coils (sampling rate 10 MHz), see Fig. 10. These modes are similar to previous observations on NSTX that were interpreted as Compressional Alfvén Eigenmodes [25] and to earlier observations on MAST using a lower data sampling rate [26].

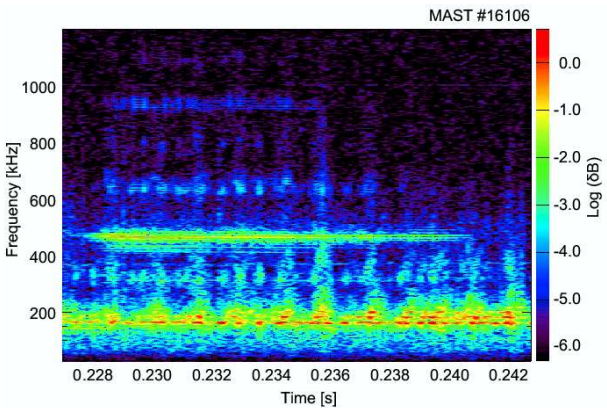

FIG. 10. High frequency MHD activity following cessation of Alfvén cascades in MAST #16105. TAE are observed at $f \sim 175$ kHz

5. Conclusions

Detailed MHD studies in MAST have helped clarify the role of plasma rotation on MHD stability; an important issue for ITER where large sawteeth may destabilise NTMs. Error field scalings for locked mode formation confirm conventional aspect ratio scalings, increasing confidence in ITER predictions. New modelling studies have shown how MAST accesses the rotationally stabilised regime that governs the β_N limit, enabling it to probe this physics and address critical questions for the AT operation of ITER and an ST power plant. The low magnetic field in MAST has identified it as an ideal test bed for fast particle driven modes and the observation of Alfvén cascades has confirmed the development of reversed magnetic shear configurations that endure well into the plasma current flat-top phase. Observations of these modes have indicated the rate of plasma current diffusion and the occurrence of rational values of the safety factor at the surface of magnetic shear reversal.

References

[1] SYKES, A. *et al. Nucl. Fusion,* **39** (1999) 1271
[2] CHAPMAN I., HUYSMANS G., SHARAPOV S. AND MIKHAILOVSKII A. *Phys. Plasmas* **13** (2006) 065211
[3] NAVE M.F.F. *et al Proc. 31st EPS Conf. Plasma Physics (London)* **28G** (2004) P1.162
[4] UDINTSEV V. *et al Plasma Phys. Control. Fusion* **47** (2005) 1111
[5] MIKHAILOVSKII A.B. & SHARAPOV S.E. *Plasma Phys. Control. Fusion* **42** (2000) 57
[6] HUYSMANS G., GOEDBLOED J. AND KERNER W, *Proc. CP90 Conf. on Comput. Phys.* **37** (1991)
[7] STRUMBERGER E. et al, *Nucl. Fusion,* **45** (2005) 1156
[8] WAELBROECK F *Phys. Plasmas* **3** (1996) 1047
[9] GRAVES J. *et al*, *Phys. Plasmas*, **10** (2003) 1034
[10] PINCHES S.D. *et al Plasma Phys. Control. Fusion* **46** (2004) S47
[11] ITER Physics Basis *Nucl. Fusion* **39** (1999) 2292
[12] SHARAPOV S.E. *et al*, *Phys. Letters A* **289** (2001) 127
[13] BERK H.L. *et al*, *Phys. Rev. Lett.* **87** (2001) 185002
[14] SHARAPOV S.E. *et al*, *Phys. Plasmas* **9** (2002) 2027
[15] SHARAPOV S.E. *et al*, *Phys. Rev. Lett.* **93** (2004) 165001
[16] VAN ZEELAND M.A. *et al*, *Plasma Physics Control. Fusion* **47** (2005) L31
[17] KIMURA H. *et al*, *Nuclear Fusion* **38** (1998) 1303
[18] NAZIKIAN R. *et al*, *Phys. Rev. Lett.* **91** (2003) 125003
[19] SNIPES J.A. *et al*, *Phys. Plasmas* **12** (2005) 056102
[20] JOFFRIN E. *et al*, *Nuclear Fusion* **43** (2003) 1167
[21] BERK H.L *et al.*, *Phys. Lett. A* **234** (1997) 213 / **238** (1998) 408 *(erratum)*
[22] GRYAZNEVICH M.P., SHARAPOV S.E., *Plasma Phys. Control. Fusion* **46** (2004) S15
[23] WILSON H.R. *et al*, *Nucl. Fusion* **44** (2004) 917
[24] PENG Y.-K.M. *et al*, *Plasma Phys. Control. Fusion* **47** (2005) B263
[25] GORELENKOV N.N *et al*, Nucl. Fusion **42** (2002) 977
[26] APPEL L.C. *et al.*, *Proc. 31st EPS Conf. Plasma Physics (London)* **28G** (2004) P4.195

This work was funded jointly by the United Kingdom Engineering and Physical Sciences Research Council and by the European Communities under the contract of Association between EURATOM and UKAEA. The views and opinions expressed herein do not necessarily reflect those of the European Commission.